Inorg. Chem. **2004**, *43*, 3930–3941

A New High-Spin Iron(III) Complex with a Pentadentate Macrocyclic Amidopyridine Ligand: A Change from Slow Single-Ion Paramagnetic Relaxation to Long-Range Antiferromagnetic Order in a Hydrogen-Bonded Network

Ivan V. Korendovych,[†] Richard J. Staples,[‡] William M. Reiff,*[,§] and Elena V. Rybak-Akimova*[,†]

Department of Chemistry, Tufts University, Medford, Massachusetts 02155, Department of Chemistry and Chemical Biology, Harvard University, Cambridge, Massachusetts 02138, and Department of Chemistry and Chemical Biology, Northeastern University, Boston, Massachusetts 02115

Received October 6, 2003

A new, stable iron(III) complex with a pentadentate amide-containing macrocyclic ligand was prepared and fully characterized. The complex adopted a pentagonal-bipyramidal geometry, where an equatorial plane is occupied by the pyridine nitrogen, two deprotonated amide nitrogens, and two secondary amines from the macrocycle, and two axial positions are available for monodentate ligand (chloride anion or solvent molecule) coordination. The rigid, planar iron–amide building blocks are linked in a three-dimensional network via a system of hydrogen bonds, with the shortest Fe–Fe separation of 8.02 Å. The coordination of strongly electron-donating, negatively charged deprotonated amide groups resulted in expected stabilization of a high oxidation state of iron (the redox potential of the $Fe^{III}L/Fe^{II}L$ couple, –0.57 V vs SCE). In contrast to the majority of the iron complexes with polydentate amide ligands, the pentagonal-bipyramidal geometry of the macrocyclic complex described in this work affords a high-spin configuration of the central metal ion (room-temperature magnetic moment is 5.84 μ_β). Variable-temperature iron-57 Mössbauer spectroscopy and ac and dc magnetization studies indicate slow paramagnetic relaxation and a crossover to long-range antiferromagnetic order at $T < \sim 3.2$ K.

Introduction

Iron complexes with amide-containing ligands provide insight concerning the structure and function of important metallobiomolecules, such as iron bleomycin[1−3] and nitrile hydratase.[4,5] Antitumor bleomycins capable of bringing about oxidative DNA cleavage are known to have an iron center coordinated to both a pyrimidine ring and an adjacent amide nitrogen.[6] Varying the structures of polydentate amide-containing ligands and probing the chemistry of the resulting iron complexes are instrumental in uncovering structure−activity relationships in bleomycin models, and in determining the details of iron−bleomycin redox chemistry. Mascharak and co-workers[7−16] and others[17−23] demonstrated

* Corresponding author. E-mail: elena.rybak-akimova@tufts.edu.
† Tufts University.
‡ Harvard University.
§ Northeastern University.

(1) Burger, R. M. *Chem. Rev.* **1998**, *98*, 1153−1169.
(2) Stubbe, J.; Kozarich, J. W.; Wu, W.; Vanderwall, D. E. *Acc. Chem. Res.* **1996**, *29*, 322−330.
(3) Hecht, S. M. *Acc. Chem. Res.* **1986**, *19*, 383−391.
(4) Huang, W.; Jia, J.; Cummings, J.; Nelson, M.; Schneider, G.; Lindqvist, Y. *Structure* **1997**, *5*, 691.
(5) Nagashima, S.; Nakasako, M.; Dohmae, N.; Tsujimura, M.; Takio, K.; Odaka, M.; Yohda, M.; Kamiya, N.; Endo, I. *Nat. Struct. Biol.* **1998**, *5*, 347.
(6) Neese, F.; Zaleski, J. M.; Loeb Zaleski, K.; Solomon, E. I. *J. Am. Chem. Soc.* **2000**, *122*, 11703−11724.
(7) Tao, X.; Stephan, D. W.; Mascharak, P. K. *Inorg. Chem.* **1987**, *26*, 754−759.
(8) Noveron, J. C.; Olmstead, M. M.; Mascharak, P. K. *Inorg. Chem.* **1998**, *37*, 1138−1139.
(9) Marlin, D. S.; Olmstead, M. M.; Mascharak, P. K. *Inorg. Chem.* **1999**, *38*, 3258−3260.
(10) Marlin, D. S.; Olmstead, M. M.; Mascharak, P. K. *Inorg. Chim. Acta* **2000**, *297*, 106−114.
(11) Noveron, J. C.; Olmstead, M. M.; Mascharak, P. K. *J. Am. Chem. Soc.* **2001**, *123*, 3247−3259.
(12) Brown, S. J.; Olmstead, M. M.; Mascharak, P. K. *Inorg. Chem.* **1990**, *29*, 3229−3234.
(13) Rowland, J. M.; Olmstead, M. M.; Mascharak, P. K. *Inorg. Chem.* **2001**, *40*, 2810−2817.
(14) Harrop, T. C.; Tyler, L. A.; Olmstead, M. M.; Mascharak, P. K. *Eur. J. Inorg. Chem.* **2003**, 475−481.

10.1021/ic0351601 CCC: $27.50
Published on Web 05/29/2004

Scheme 1

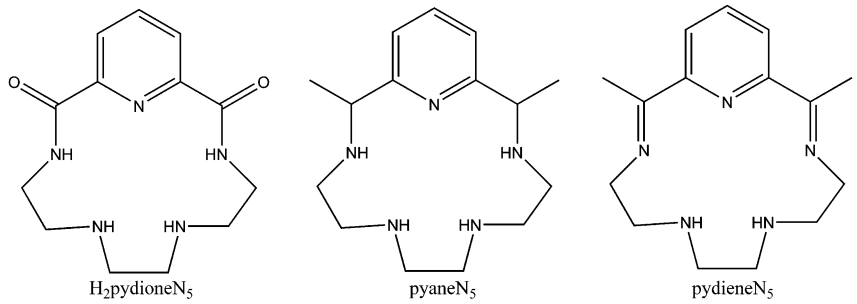

that deprotonated amides are good ligands for iron(III), forming stable complexes. Several iron complexes with amide ligands are catalytically active in oxidation reactions.[16,24,25]

Due to the strong σ-donor properties of negatively charged, electron-rich amide ligands, the vast majority of their iron(III) complexes contain a low-spin metal center.[7−9,11−18,26] Controlling the spin state of iron is important in modulating the redox reactivity of iron complexes.[27] It was recently demonstrated that replacing one or two (out of five) nitrogen donor atoms with phenolate donors gives rise to high-spin ferric amidates.[10,15] While these results are certainly interesting and promising, it is desirable to gain control over the spin state of iron without changing the nature of the donor atoms so dramatically. We decided to explore the role of iron coordination geometry in determining the spin state and redox properties of ferric complexes with pentadentate, N_5 diamides.

This paper describes the synthesis and characterization of new iron(III) complex with a pentadentate macrocyclic ligand, H_2pydioneN_5 (Scheme 1). The cyclic nature of the ligand substantially reduces its flexibility and ensures that the complexes retain their solid-state structures in solution. Pentadentate pentaaza macrocycles pyaneN_5 and pydieneN_5 (Scheme 1) are known to occupy an equatorial plane in pentagonal-bipyramidal complexes in which two additional monodentate ligands (such as halides or pseudohalides) coordinate axially.[28−33] These pentagonal bipyramidal iron(III) complexes with pyaneN_5 and pydieneN_5 were shown to be high-spin.[30,31] We hypothesized that five in-plane donors of amide-containing pydioneN_5 would also favor the high-spin state of iron(III).

Incorporation of two amide groups into the macrocyclic framework is expected to substantially modulate the electronic structure of the central iron(III) ion and to provide new opportunities for intermolecular interactions. The amide donors are known to stabilize high oxidation states of the coordinated metal ions.[24,34−37] We set out to explore the effect of two amide groups in pentaaza macrocyclic environment on redox properties of their iron complexes. Additionally, the presence of exocyclic amide carbonyl oxygen atoms that can act as hydrogen bond acceptors allows for the formation of three-dimensional networks. Amide complexes are useful building blocks for supramolecular architectures.[38−41] In recent years, interesting magnetic properties of three-dimensional metal-organic frameworks[38,42] attracted attention as a basis for designing molecular magnets.[43−45] Even though magnetic coupling through hydrogen bonds is relatively weak,[41,46−48] H-bonded three-dimensional networks were reported to undergo magnetic ordering at low temperatures

(15) Marlin, D. S.; Olmstead, M. M.; Mascharak, P. K. *Eur. J. Inorg. Chem.* **2002**, 859−865.
(16) Guajardo, R. J.; Hudson, S. E.; Brown, S. J.; Mascharak, P. K. *J. Am. Chem. Soc.* **1993**, *115*, 5.
(17) Che, C.-M.; Leung, W.-H.; Li, C.-K.; Cheng, H.-Y.; Peng, S.-M. *Inorg. Chim. Acta* **1992**, *196*, 43−48.
(18) Ray, M.; Ghosh, D.; Shirin, Z.; Mukherjee, R. *Inorg. Chem.* **1997**, *36*, 3568−3572.
(19) Ray, M.; Mukherjee, R.; Richardson, J. F.; Buchanan, R. M. *J. Chem. Soc., Dalton Trans.* **1993**, 2457.
(20) Kostka, K. L.; Fox, B. G.; Hendrich, M. P.; Collins, T. J.; Rickard, C. E. F.; Wright, L. J.; Munck, E. *J. Am. Chem. Soc.* **1993**, *115*, 6746−6757.
(21) Bartos, M. J.; Kidwell, C.; Kauffmann, K. E.; Gordon-Wylie, S. W. *Angew. Chem., Int. Ed. Engl.* **1995**, *34*, 1216.
(22) Heinrich, L.; Li, Y.; Vaussermann, J.; Chottard, G.; Chottard, J. C. *Angew. Chem., Int. Ed.***1999**, *38*, 3526.
(23) Artaud, I.; Chatel, S.; Chauvin, A. S.; Bonnet, D.; Kopf, M. A.; Leduc, P. *Coord. Chem. Rev.* **1999**, *190−192*, 577.
(24) Collins, T. J. *Acc. Chem. Res.* **1994**, *27*, 279−285.
(25) Nguen, C.; Guajardo, R. J.; Mascharak, P. K. *Inorg. Chem.* **1996**, *35*, 5.
(26) Zhu, S.; Brennessel, W. W.; Harrison, R. G.; Que, L., Jr. *Inorg. Chim. Acta* **2002**, *337*, 32−38.
(27) Fujita, M.; Costas, M.; Que, L., Jr. *J. Am. Chem. Soc.* **2003**, *125*, 9912−9913.
(28) Nelson, M.; Bryan, P.; Busch, D. H. *Chem. Commun.* **1966**, 641.
(29) Fleischer, E. B.; Hawkinson, S. W. *J. Am. Chem. Soc.* **1967**, *89*, 720−721.
(30) Nelson, M.; Busch, D. H. *Inorg. Chem.* **1969**, *8*, 1859−1863.
(31) Rakowski, M. C.; Rycheck, M.; Busch, D. H. *Inorg. Chem.* **1975**, *14*, 1194−1200.
(32) Drew, M. G. B.; bin Othman, A. H.; McIlroy, P. D. A.; Nelson, S. M. *J. Chem. Soc. Dalton* **1975**, 2507−2516.
(33) Drew, M. G. B.; Rice, D. A.; Bin Silong, S. *Polyhedron* **1983**, *2*, 1053−1056.
(34) Rybka, J. S.; Margerum, D. W. *Inorg. Chem.* **1981**, *20*, 1453−1458.
(35) Rybka, J. S.; Margerum, D. W. *Inorg. Chem.* **1980**, *19*, 2784−2790.
(36) Gavrish, S. P.; Lampeka, Y. D. *J. Coord. Chem.* **1991**, *24*, 351−362.
(37) Bartos, M. J.; Gordon-Wylie, S. W.; Fox, B. G.; James Wright, L.; Weintraub, S. T.; Kauffmann, K. E.; Münck, E.; Kostka, K. L.; Uffelman, E. S.; Rickard, C. E. F.; Noon, K. R.; Collins, T. J. *Coord. Chem. Rev.* **1998**, *174*, 361−390.
(38) Braga, D.; Grepioni, F.; Desiraju, G. R. *Chem. Rev.* **1998**, *98*, 1375−1406.
(39) Ruiz, R.; Faus, J.; Lloret, F.; Julve, M.; Journaux, Y. *Coord. Chem. Rev.* **1999**, *193−195*, 1069−1117.
(40) Burkill, H. A.; Vilar, R.; White, A. J. P.; Williams, D. J. *J. Chem. Soc., Dalton Trans.* **2002**, 837−839.
(41) Tercero, J.; Diaz, C.; Ribas, J.; Ruiz, E.; Mahia, J.; Maestro, M. *Inorg. Chem.* **2002**, *41*, 6780−6789.
(42) Janiak, C. *Dalton Trans.* **2003**, 2781−2804.
(43) Kahn, O. Ed. *Magnetism: A Supramolecular Function*; Kluwer Academic Publishers: Dordrecht, The Netherlands, 1996.
(44) Kahn, O. *Adv. Inorg. Chem.* **1996**, *43*, 179.
(45) Neese, F.; Solomon, E. I. In *Magnetism: Molecules to Materials IV*; Miller, J. S., Drillon, M., Eds.; Wiley: New York, 2003; pp 345−466.

(some examples can be found in refs 41 and 49−54). Therefore, magnetic properties of new amide-containing, potentially high-spin iron(III) macrocycles were explored in detail in the present study.

Experimental Section

General. ^{1}H (300.35 MHz) and ^{13}C (75.53 MHz) NMR spectra were recorded on a Bruker DPX-300 spectrometer and referenced to the residual solvent peak (^{1}H $\delta(CHCl_3) = 7.27$ ppm) or to the solvent peak (^{13}C $\delta(CDCl_3) = 77.23$ ppm). UV−visible spectra were recorded over the 200−1100 nm range on a Hitachi U-2000 spectrometer. Variable temperature UV−vis studies were performed with PC2000 CCD array spectrometer equipped with a TP300−UV−Vis Transflection Dip Probe (Ocean Optics Inc.) over the 350−800 nm range using a modified setup described by Rivera et al.[55] IR spectra were recorded in KBr pellets on a Mattson 1000 FTIR spectrometer at a 2 cm^{-1} resolution. Electrospray mass spectrometry was performed on a HP 5989B instrument. Elemental analysis was performed at Schwarzkopf Microanalytical Laboratory (Woodside, NY).

Electrochemical Experiments. The cyclic voltammetry (CV) experiments were done under an argon atmosphere in dry dimethyl sulfoxide or dry dimethylformamide (0.1 M Tetra-*n*-butylammonium perchlorate was used as supporting electrolyte) with an EG&G PAR 273 potentiostat using a three-electrode cell with a pyrolytic graphite disk working electrode and platinum wire counter and reference electrodes. The electrolyte was thoroughly degassed prior to each experiment. Potentials were determined using ferrocene as an internal standard and are reported relative to Saturated Calomel Electrode (SCE). The following procedure was employed in order to recalculate observed potentials versus $Cp_2Fe^{+/0}$ to potentials versus SCE. Under the same experimental conditions potentials of $Cp_2Fe^{+/0}$ couple were measured in DMF and DMSO using a three electrode cell with a pyrolytic graphite disk working electrode, platinum wire as a counter electrode and SCE as a reference electrode. The potentials of $Cp_2Fe^{+/0}$ couple were found to be +0.524 V and +0.44 V versus SCE in DMF and DMSO, respectively. A conversion coefficient based on these values was applied to potentials versus $Cp_2Fe^{+/0}$ couple.

EPR Experiments. X-band EPR spectra were recorded on a Bruker EMX spectrometer either in frozen 1:1 methanol/ethanol solution or in polycrystalline form. EPR measurements in the temperature range from 4.2 to 40 K were performed at Bruker Biospin (Billerica, MA) using an ER 4112HV low-temperature control system equipped with an Oxford Instruments ESR900 helium flow Cryostat. Experiments were conducted under non-saturating conditions. Intensities of the signals were estimated from double integrals of EPR spectra and referenced to the intensities of a standard (Fe^{3+}-EDTA) measured at the same temperatures. Frozen solution EPR data were simulated using a program by Frank Neese.[56] No attempt was made to model inhomogeneous distribution of E/D ("E/D strain");[57] therefore, the EPR spectrum of **2** (Figure S1, Supporting Information) was simulated independently for two regions (600−3000 and 3000−6600 G) using the same E/D ratio of 0.08 but different effective line widths.

Mössbauer and Magnetic Susceptibility Studies. Direct current (dc) and alternating current (ac) magnetic susceptibility measurements were made on polycrystalline powder samples using a Quantum Design (MPMSXL) SQUID magnetometer at Northeastern University. Magnetic susceptibilities were corrected for the background signal of the sample holder and for diamagnetic susceptibilities of all atoms. Ac susceptometry measurements were made using a Lake Shore Cryotronics Co. Model 7000 ac susceptometer at Northeastern University. Ac measurements on powdered samples were made over the temperature range from 1.8 to 30 K in an ac field of 1 Oe amplitude at a frequency of 125 Hz and for higher temperatures at 2.5 Oe, 500 Hz.

Theoretical dependence of magnetic susceptibility on temperature for the rhombically distorted $S = 5/2$ paramagnet was calculated using the following procedure. The molar paramagnetic magnetization was calculated using[58]

$$M_a = N_A \frac{\sum_i \left(-\frac{\partial \epsilon_i}{\partial B_a}\right) \exp\left(-\frac{\epsilon_i}{kT}\right)}{\sum_i \exp\left(-\frac{\epsilon_i}{kT}\right)} \quad (1)$$

where $a = x$, y, or z, k is the Boltzmann constant, ϵ_i are the energy levels of the spin states, B_a is the magnetic induction along the a axis, and T is the temperature. The values of zero-field splitting and rhombic distortion were taken from the EPR data ($D = -0.5$ cm^{-1}, $E/D = 0.08$); the g-tensor was presumed to be isotropic with $g = 2.00$. Field dependence of the energy levels was obtained from classical spin Hamiltonian[59]

$$H = g\beta BS + D[S_z^2 - S(S+1)/3] + E[S_x^2 - S_y^2] \quad (2)$$

Components of magnetic susceptibility were calculated from

$$\chi_a = \mu_0 \frac{M_a}{B_a} \quad (3)$$

And the powder magnetic susceptibility is given by

$$\chi = \frac{1}{3}(\chi_x + \chi_y + \chi_z) \quad (4)$$

Calculations were done using Mathcad 2000i Professional software. The Mathcad worksheet for magnetic susceptibility calculations can be obtained from the authors upon request.

(46) Desplanches, C.; Ruiz, E.; Rodriguez-Fortea, A.; Alvarez, S. *J. Am. Chem. Soc.* **2002**, *124*, 5197−5205.
(47) De Munno, G.; Ventura, W.; Viau, G.; Lloret, F.; Faus, J.; Julve, M. *Inorg. Chem.* **1998**, *37*, 1458−1464.
(48) Galan-Mascaros, J.-R.; Clemente-Juan, J.-M.; Dunbar, K. R. *Dalton Trans.* **2002**, 2710−2713.
(49) Armentano, D.; De Munno, G.; Lloret, F.; Palii, A. V.; Julve, M. *Inorg. Chem.* **2002**, *41*, 2007−2013.
(50) Martinez Lorente, M. A.; Dahan, F.; Petrouleas, V.; Buousseksou, A.; Tuchagues, J.-P. *Inorg. Chem.* **1995**, *34*, 5346−5357.
(51) Van Langenberg, K.; Batten, S. R.; Berry, K. J.; Hockless, D. C. R.; Moubaraki, B.; Murray, K. S. *Inorg. Chem.* **1997**, *36*, 5006−5015.
(52) Price, D. J.; Batten, S. R.; Moubaraki, B.; Murray, K. S. *Polyhedron* **2003**, *22*, 2161−2167.
(53) Liu, T.-F.; Sun, H.-L.; Gao, S.; Zhang, S.-W.; Lau, T.-C. *Inorg. Chem.* **2003**, *42*, 4792−4794.
(54) Kahn, O.; Larionova, J.; Yakhmi, J. V. *Chem. Eur. J.* **1999**, *5*, 3443−3449.
(55) Rivera, M.; Caignan, G. A.; Astashkin, A. V.; Raitsimring, A. M.; Shokhireva, T. K.; Walker, F. A. *J. Am. Chem. Soc.* **2002**, *124*, 6077−6089.
(56) Neese, F. The Program EPR. *QCPE Bull.* **1995**, *15*, 5.
(57) Neese, F.; Solomon, E. I. *J. Am. Chem. Soc.* **1998**, *120*, 12829−12848.
(58) Boca, R. *Theoretical Foundation of Molecular Magnetism*; Elsevier: Amsterdam, 1999; Vol. 1.
(59) Trautwein, A. X.; Bill, E.; Bominaar, E. L.; Winkler, H. *Struct. Bonding* **1991**, *78*, 1−95.

The Mössbauer spectra were determined using a conventional constant acceleration spectrometer operated in multichannel scaling mode. The γ ray source consisted of 51 mCi of ^{57}Co in a rhodium metal matrix that was maintained at ambient temperature. The spectrometer was calibrated using a 6 μm thick natural abundance iron foil. Isomer shifts are reported relative to the center of the magnetic hyperfine pattern of the latter foil taken as zero velocity. The line widths of the innermost pair of $\Delta M_I = \pm 1$ transitions of the latter Zeeman pattern were reproducibly determined to be 0.214 mm/s. Sample temperature variation was achieved using a standard exchange gas liquid helium cryostat (Cryo Industries of America, Inc.) with temperature measurement and control based on silicon diode thermometry in conjunction with a 10 μAmp excitation sources (Lakeshore Cryotronics, Inc). To determine δ and ΔE_Q, spectra were fit to unconstrained Lorentzians using the program ORIGIN PRO V 7.0 (Originlab, Inc.)

HPLC. HPLC experiments were performed on HP 1050 instrument using 10 cm × 4.6 mm 5μm SUPELCOSIL LC-18 column with acetonitrile (A) and water (B), both containing 0.2% TFA, as mobile phases. Gradient elution from 10% to 90% (A) was employed during a 10 min run.

Materials. All materials used were ACS reagent-grade or better and were used without additional purification. Anhydrous iron(III) chloride was purchased from Strem Chemicals. 2,6-Pyridinedicarboxylic acid and anhydrous dimethyl sulfoxide were purchased from Acros. All other reagents were purchased from Aldrich. 2,6-Pyridinedicarboxylic acid dimethyl ester was synthesized according to the published procedure.[60] 1,4,7,10-Tetraazadecane was dried over KOH at 60 °C and was distilled over sodium prior to use.

Syntheses. H_2pydioneN_5 (1). The ligand **1** was obtained according to the published procedure.[60] The compound can be additionally purified by recrystallization from boiling acetonitile. Yields normally range from 15% to 40%. HPLC retention time was 3.2 min. ^{1}H NMR (300 MHz, $CDCl_3$) δ 9.13 (t, $J = 5.9$ Hz, 2H, −C(O)N*H*-), 8.25 (d, $J = 7.7$, 2H, β-H of the pyridine ring), 8.0 (t, $J = 7.7$ Hz, 1H, γ-H of the pyridine ring), 3.51 (q, $J = 5.2$ Hz obs., 4H, −C(O)NHCH_2−), 2.96 (t, $J = 5.5$ Hz, 4H, −C(O)-NHCH$_2$CH_2-), 2.85 (s, 4H, −CH$_2$NHCH_2CH_2NHCH$_2$−), 1.2 (br, 2H, −CH$_2$N*H*CH$_2$−). ^{13}C NMR (75 MHz, $CDCl_3$) δ 163.0 (2C), 148.7 (2C), 139.3 (1C), 123.7 (2C), 49.4 (2C), 47.6 (2C), 39.0 (2C). MS (ESI), *m*/z: 278.1 (100%, $[M+H]^+$). UV−vis (MeOH) λ_{max}, nm (ϵ, $M^{-1}cm^{-1}$) 204 (12400); 224 (8600); 272 sh. (3360).

Selected FTIR absorption bands (KBr pellet, ν/cm^{-1}): 3365−3297 (m, ν N−H); 3080 (m, ν C_{pyr}−H); 2950−2815 (m, ν C−H); 1677 (vs, ν C═O); 1589, 1446 (m,s $\nu_{\text{pyridine ring}}$); 1523 (s, ν C−N).

[Fe(pydioneN_5)Cl(H_2O)](MeOH) (2). In a glovebox, a solution of 277 mg (1 mmol) of **1** in 4 mL of dry methanol was slowly added to a vigorously stirred solution of 161 mg (1 mmol) of anhydrous iron(III) chloride in 3 mL of dry methanol. Triethylamine (202 mg, 0.28 mL, 2 mmol) was added to this mixture to give an intensely colored orange solution of **2**. Formation of precipitate was sometimes observed at this stage. The precipitate, if formed, redissolved within few days to give solution of **2**. Upon exposure to air solid **2** crystallized within 3 days and can be additionally purified by recrystallization from methanol. The presence of water during the initial reaction significantly decreases yield of the product. Yield: 350 mg (84%). UV−vis (MeOH), λ_{max}, nm (ϵ, M^{-1} cm^{-1}): 244 (10600); 262 sh. (9500); 461 (1400). MS (ESI), *m*/z: 367.0 $[M+H]^+$; 331.1 (100%, $[M-Cl]^+$). Selected FTIR absorption bands (KBr pellet, ν/cm^{-1}): 2950−2815 (m, ν C−H); 1621 (vs, ν C═O); 1590, 1442 (m,s $\nu_{\text{pyridine ring}}$); 1561 (s, ν C−N). Anal. Calcd for $C_{14}H_{23}ClFeN_5O_4$: C, 40.36; H, 5.56; N, 16.81; Fe, 13.40. Found: C, 37.40; H, 5.64; N, 16.76; Fe, 13.54. Phase purity of compound **2** was additionally confirmed by X-ray powder diffraction studies. Data were acquired on Bruker D8 Discover diffractometer with GADDS detector using Cu K_α radiation. Comparison of calculated and observed reflections is given in Table S1 (Supporting Information).

Table 1. Crystallographic Data for **1** and **2**

chemical formula	$C_{13}H_{19}N_5O_2$ (**1**)	$C_{14}H_{23}ClFeN_5O_4$ (**2**)
formula weight	277.33	416.67
space group	*C*2/*c*	$P2_1/c$
a, Å	13.9346(18)	11.5958(13)
b, Å	11.3632(14)	11.4695(13)
c, Å	17.801(2)	14.5979(16)
α, deg	90	90
β, deg	95.632(3)	108.303(2)
γ, deg	90	90
V, Å^3	2805.0(6)	1843.3(4)
Z	8	4
T, K	213(2)	213(2)
λ, Å	0.71073	0.71073
D_{calcd}, g cm^{-3}	1.313	1.501
μ, mm^{-1}	0.093	0.992
final *R* indices[a]	$R = 0.0520$	$R = 0.0647$
[$I > 2\sigma(I)$]	$wR_2 = 0.1574$	$wR_2 = 0.1525$
final *R* indices[a]	$R = 0.0671$	$R = 0.0748$
[for all data]	$wR_2 = 0.1648$	$wR_2 = 0.1576$

[a] $R = \sum||F_o| - |F_c||/\sum|F_o|$. $wR_2 = \{\sum[w(F_o^2 - F_c^2)^2]/\sum[w(F_o^2)^2]\}^{1/2}$.

X-ray Crystallographic Data. Data were collected using a Bruker SMART CCD (charge coupled device) based diffractometer equipped with an LT-3 low-temperature apparatus operating at 213 K. A suitable crystal was chosen and mounted on a glass fiber using grease. Data were measured using ω scans of 0.3° per frame for 30 s, such that a hemisphere was collected. A total of 1271 frames were collected with a maximum resolution of 0.75 Å. The first 50 frames were recollected at the end of data collection to monitor for decay. Cell parameters were obtained using SMART software[61] and refined using SAINT[62] on all observed reflections. Data reduction was performed using the SAINT software[62] which corrects for Lorentz polarization effects and compound decomposition. No compound decomposition was observed. Absorption corrections were applied using SADABS.[63] The structures were solved by the direct method using the SHELXS-97 program[64] and refined by least-squares method on F^2, SHELXL-97,[65] incorporated in SHELXTL-PC V 5.10.[66] All drawing are done at 50% ellipsoids.

The structure of **1** was solved in the space group $P2_1/c$ (No. 14) and the structure of **2** in the space group *C*2/*c* (No. 15) by analysis of systematic absences. All non-hydrogen atoms were refined anisotropically. Hydrogens were calculated by geometrical methods and refined with a riding model. The crystals used for the diffraction study showed no decomposition during data collection. Crystal data collection and refinement parameters for **1** and **2** are given in Table 1.

(60) Dierck, I.; Herman, G. G.; Goeminne, A. M.; Van der Kelen, G. P. *Bull. Soc. Chim. Belg.* **1993**, *102*, 63−66.

(61) *SMART V 5.050 (NT) Software for the CCD Detector System*; Bruker Analytical X-ray Systems: Madison, WI, 1998.

(62) *SAINT V 5.01 (NT) Software for the CCD Detector System*; Bruker Analytical X-ray Systems: Madison, WI, 1998.

(63) Sheldrick, G. M. *SADABS*; University of Göttingen: Göttingen, Germany, 1996.

(64) Sheldrick, G. M. *SHELXS-90, Program for the Solution of Crystal Structure*; University of Göttingen: Göttingen, Germany, 1990.

(65) Sheldrick, G. M. *SHELXL-97, Program for the Refinement of Crystal Structure*; University of Göttingen: Göttingen, Germany, 1997.

(66) *SHELXTL 5.10 (PC-Version) Program library for Structure Solution and Molecular Graphics*. Bruker Analytical X-ray Systems: Madison, WI, 1998.

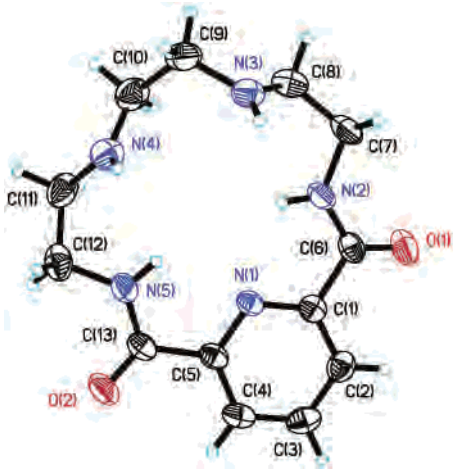

Figure 1. Crystal structure of **1**.

Results and Discussion

Amidopyridine macrocycle H_2pydioneN_5 (Scheme 1) and its analogues have been prepared previously,[60,67,68] but its complexation with transition metal ions has not been studied. We found that anhydrous iron(III) chloride readily reacts with H_2pydioneN_5 at ambient temperature in the presence of 2 equiv of triethylamine, yielding an iron(III) complex with a doubly deprotonated ligand, [Fe(pydioneN_5)Cl(H_2O)]. The yields of the iron(III) complex decrease significantly in the presence of trace amounts of water in the reaction mixture. The isolated complex, however, is air- and water-stable both in the solid state and in solutions. Aqueous solutions of this complex can be prepared and do not undergo decomposition for days. Furthermore, the complex is stable in aqueous solution in the presence of a 10-fold excess of EDTA. The spectroscopic, structural, and magnetic properties of the complex [Fe(pydioneN_5)Cl(H_2O)] indicate that the central metal ion is in the high-spin state (see discussion below).

Structural Features. Both the free ligand H_2pydioneN_5 (**1**) and its iron(III) complex [Fe(pydioneN_5)Cl(H_2O)]-(MeOH) (**2**) were structurally characterized, thus allowing for informative comparison of their structural features.

A view of the X-ray structure of the free ligand is presented in Figure 1, and selected bond lengths and angles are given in Table 2. All five nitrogen atoms of the ligand lie essentially in a plane (mean deviation of atoms from the plane is 0.12 Å). Both amide groups are not coplanar with the pyridine ring: the average angle between the plane of the pyridine ring and the plane of the amide group is 12°. This deviation from the lowest energy state when the amide groups are conjugated with the pyridine ring apparently occurs due to the steric hindrance caused by the relatively small size of the macrocyclic ring. Structural parameters of the amide groups are as follows: average C═O distance is 1.23 Å, the C−N distance is 1.32 Å, and the $C_{amide}-C_{pyr}$ distance is 1.51 Å.

Table 2. Selected Bond Lengths (Å) and Angles (deg) for **1** and **2**

	1	**2**
N(2)−C(6)	1.326(2)	1.305(7)
N(2)−C(7)	1.4472(19)	1.465(7)
N(5)−C(13)	1.319(2)	1.305(7)
N(5)−C(12)	1.437(2)	1.466(7)
C(1)−C(6)	1.509(2)	1.485(7)
C(5)−C(13)	1.507(2)	1.501(7)
O(1)−C(6)	1.2285(19)	1.271(6)
O(2)−C(13)	1.2326(17)	1.270(6)
Fe(1)−O(3)		2.041(3)
Fe(1)−N(2)		2.155(4)
Fe(1)−N(5)		2.156(4)
Fe(1)−N(1)		2.193(4)
Fe(1)−N(3)		2.269(4)
Fe(1)−N(4)		2.279(4)
Fe(1)−Cl(1)		2.3573(13)
C(6)−N(2)−C(7)	126.24(14)	117.0(4)
C(13)−N(5)−C(12)	127.01(14)	116.9(4)
O(2)−C(13)−C(5)	121.26(15)	127.3(5)
N(5)−C(13)−C(5)	114.34(13)	112.7(4)
O(3)−Fe(1)−N(2)		85.99(14)
O(3)−Fe(1)−N(5)		92.08(15)
O(3)−Fe(1)−N(1)		91.93(14)
N(2)−Fe(1)−N(1)		71.49(15)
N(5)−Fe(1)−N(1)		71.26(15)
O(3)−Fe(1)−N(3)		88.45(14)
N(2)−Fe(1)−N(3)		72.52(16)
O(3)−Fe(1)−N(4)		85.54(14)
N(5)−Fe(1)−N(4)		71.98(16)
N(3)−Fe(1)−N(4)		73.00(16)
O(3)−Fe(1)−Cl(1)		174.39(11)
N(4)−Fe(1)−Cl(1)		91.38(11)
C(6)−N(2)−Fe(1)		122.0(3)
C(7)−N(2)−Fe(1)		120.4(3)
C(13)−N(5)−C(12)		116.9(4)
C(13)−N(5)−Fe(1)		122.6(3)
C(12)−N(5)−Fe(1)		120.5(3)
O(1)−C(6)−N(2)	125.22(15)	127.8(5)
O(1)−C(6)−C(1)	120.68(15)	119.1(5)
N(2)−C(6)−C(1)	114.07(13)	113.0(4)
N(2)−C(7)−C(8)	108.54(14)	107.1(4)
N(5)−C(12)−C(11)	107.86(14)	107.8(5)
O(2)−C(13)−N(5)	124.38(16)	127.3(5)
O(3)−H(3B)···O(1)		2.581
O(2)−H(3A)···O(3)		2.610
O(1S)−H(1S)···O(2)		2.827
N(4)−(H3C)···O(1)		2.901

The structure of the Fe^{III} complex of **1** is shown in Figure 2, and selected bond lengths and angles are given in Table 2. The coordination sphere of iron(III) consists of the five nitrogen atoms of the macrocycle, forming an almost perfect plane (mean deviation of the atoms from the plane defined through N(1), N(2), N(3), N(4), N(5), and Fe(1) is 0.06 Å), and coordinated chloride and water in the axial positions. The coordination polyhedron of the iron(III) is an almost perfect pentagonal bipyramid: all angles N−Fe−N are 72 ± 1°, all angles N_{eq}−Fe−Cl(1) and N_{eq}−Fe−O(3) are 90 ± 5°, and the angle Cl(1)−Fe−O(3) is 174.4°.

The average Fe−N_{amido} bond length of 2.156 Å is consistent with the usual high-spin Fe^{III}−N_{amido} bond distance of 2.06−2.23 Å.[69] This is considerably longer than the Fe−N_{amido} bond (1.95−1.97 Å) in low-spin complexes containing 2,6-bisamidopyridine fragment.[9,18] However, the size of the macrocyclic cavity might influence geometric parameters of **2** as well. Indeed, iron(III) complexes with pyridine-

(67) Alcock, N. W.; Moore, P.; Omar, H. A. A.; Reader, C. J. *J. Chem. Soc., Dalton Trans.* **1987**, 2643−2648.
(68) Rorrer, L. C.; Hopkins, S. D.; Connors, M. K.; Lee, D. W., III; Smith, M. V.; Rhodes, H. J.; Uffelman, E. S. *Org. Lett.* **1999**, *1*, 1157−1159.
(69) Marlin, D. S.; Mascharak, P. K. *Chem. Soc. Rev.* **2000**, *29*, 69−74.

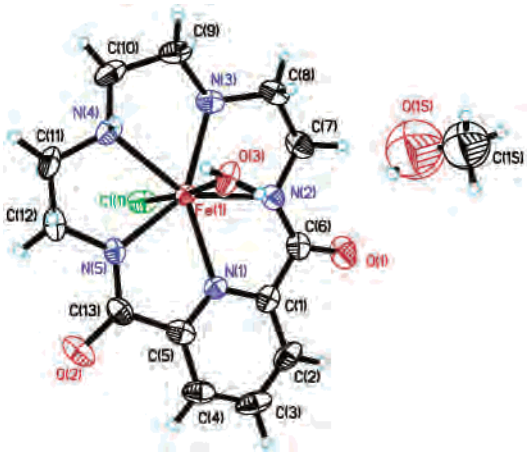

Figure 2. Crystal structure of **2**.

Scheme 2. Resonance Structures of the Coordinated Amidopyridine Fragment

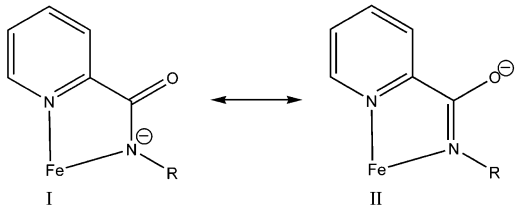

containing pentaaza macrocycles display a very similar geometry of the metal coordination sphere. Several crystal structures of iron(III) complexes with closely related macrocyclic ligands, $[Fe(pyaneN_5)Cl_2](PF_6)$[33] and $[Fe(pydieneN_5)(NCS)_2](ClO_4)$,[32] have been reported. The size of the macrocyclic hole in **2** (determined by a method described by Tasker et al [70]) is 4.42 Å compared to 4.45 Å in the iron(III) complex with pydieneN_5 and 4.50 Å in the iron(III) complex with pyaneN_5. The shrinking of the macrocyclic hole is mostly determined by short Fe−N_{amido} bonds (2.156 Å) compared to Fe−N_{schiff} bonds (2.25 Å)[32] and Fe−N_{amine} bonds (2.25 Å).[33] Axial Fe−Cl bond distances in $[Fe(pydioneN_5)Cl(H_2O)]$ and $[Fe(PyaneN_5)Cl_2]^+$ are essentially the same (2.35 Å), which suggests that deprotonated amide groups incorporated into the equatorial macrocyclic ligand exert relatively low influence on monodentate axial ligands.

The geometry of the amide group in H_2pydioneN_5 changes substantially upon its coordination to the metal: the average C_{amide}−N distance decreases to 1.31 Å, and the average C_{amide}=O distance increases to 1.27 Å. Upon coordination to iron(III), the average angle between the plane of the pyridine ring and the plane of the amide group decreases to 3°. This can be explained by the increased degree of conjugation of the deprotonated amide with the aromatic ring due to the increased contribution from resonance structure II (Scheme 2) upon coordination of metal. This observation agrees well with the previous studies of coordination of deprotonated amide groups.[71−73]

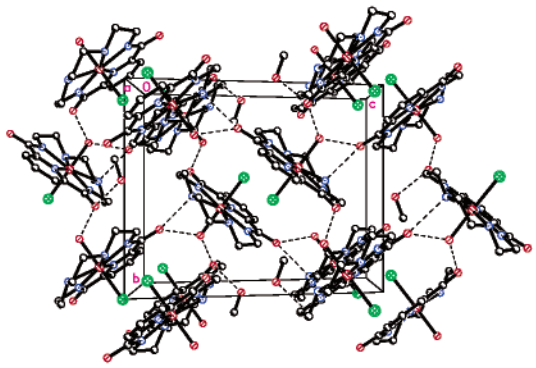

Figure 3. Packing diagram of **2** showing three-dimensional structure formed via hydrogen bonding.

In the solid state the molecules of complex **2** are connected to each other via a system of hydrogen bonds, forming a three-dimensional network (Figure 3) with the shortest iron−iron distance of 8.02 Å. One hydrogen-bonding pathway occurs through H-bonds between the coordinated water molecule and the amide oxygen atom of the neighboring iron-containing macrocycle. There is an additional interaction between the secondary amine nitrogen atom and the amide oxygen atom. A methanol molecule present in the crystal lattice is also hydrogen-bound to the oxygen atom of the amide group. Parameters of the hydrogen bonding are given in Table 2. These three-dimensional intermolecular interactions between the metal atoms may lead to cooperative effects for solid **2** (vide infra).

Spectroscopic and Redox Properties. Coordination of an amide-containing ligand to a metal can be characterized by the shift in the IR frequencies of the amide group. The shift of the amide I band from 1670 cm^{-1} in the free ligand **1** to 1621 cm^{-1} in the iron(III) complex **2** shows a decrease in the bond order of the carbonyl bond. At the same time, the shift of the amide II band from 1523 to 1561 cm^{-1} shows an increase in the double bond character of C_{amide}−N bond.[74,75] On the basis of that, it appears that upon binding of a deprotonated amide nitrogen there is a significant contribution of the resonance structure II (Scheme 2).[72,73] The shifts in vibrational frequencies of H_2pydioneN_5 upon coordination to iron(III) are consistent with a decrease in average C_{amide}−N bond length and a concomitant increase in average C_{amide}=O bond length in complex **2** as compared to free ligand **1** (Table 2).

The UV−visible spectrum of **2** is presented in Figure S2 (Supporting Information). The orange color of the complex is determined by a ligand-to-metal charge transfer (LMCT) band with a maximum at 461 nm (ϵ = 1400 M^{-1} cm^{-1}) in methanol. The position of the band is quite typical for iron(III) complexes containing a 2,6-bisamidopyridine fragment.[9,18] Interestingly, the position of the maximum of the charge-transfer band is temperature-dependent (Supporting

(70) Drummond, L. A.; Henrick, K.; Kanagasundaram, M. J. L.; Lindoy, L. F.; McPartlin, M.; Tasker, P. A. *Inorg. Chem.* **1982**, *21*, 3923−3927.
(71) Sigel, H.; Martin, R. B. *Chem. Rev.* **1982**, *82*, 385−426.
(72) Patra, A. K.; Ray, M.; Mukherjee, R. *Inorg. Chem.* **2000**, *39*, 652−657.
(73) Patra, A. K.; Mukherjee, R. *Inorg. Chem.* **1999**, *38*, 1388−1393.
(74) Mohamadou, A.; Gerard, C. *J. Chem. Soc., Dalton Trans.* **2001**, 3320−3328.
(75) Jubert, C.; Mohamadou, A.; Gerard, C.; Brandes, S.; Tabard, A.; Barbier, J.-P. *J. Chem. Soc., Dalton Trans.* **2002**, 2660−2669.

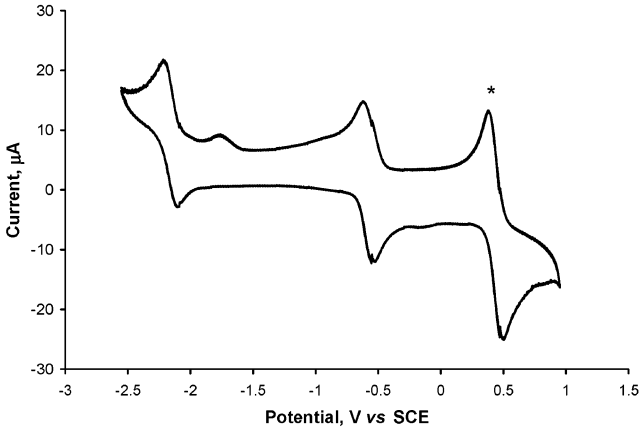

Figure 4. Cyclic voltammograms of **2** recorded in dry DMSO at scan rate of 25 mV/s (* represents the ferrocenium/ferrocene couple).

Information, Figure S3): the band maximum shifts to 435 nm at −80 °C. This thermochromic behavior cannot be attributed to changes in the spin state of iron upon cooling, as the complex remains high-spin even at liquid helium temperature (see below).

The electrochemical behavior of **2** has been studied in DMSO (Figure 4) and in DMF. The reduction of iron(III) to iron(II) occurs at −0.57 V versus SCE. As evidenced by a i_{pa}/i_{pc} of 0.89 ± 0.04, peak separation of 82 mV, and linear variation of i_p with $v^{1/2}$ (Supporting Information, Figures S4, S5), the process is reversible. The quasi reversible redox process at −2.17 and −2.05 V in DMSO and DMF, respectively, can be attributed to the reduction of the coordinated ligand. Free ligand H_2pydioneN_5 shows quasi reversible (i_{pa}/i_{pc} = 0.63) reduction in DMF at −1.96 V versus SCE (Supporting Information, Figure S6).

The effects of the amide bond coordination on the redox properties of iron complexes can be demonstrated by comparison of the electrochemical data for [Fe(pydioneN_5)-Cl(H_2O)] with the data for similar macrocycles having amino or imino groups in place of deprotonated amides. Busch et al.[31] reported that the complex [Fe(pyaneN_5)Cl_2]$^+$ exhibited an Fe^{3+}/Fe^{2+} redox process at −0.26 V versus SCE, and Ferraudi[76] obtained a value of −0.08 V versus SCE for [Fe(pydieneN_5)Cl_2]$^+$ (both redox potentials were measured in acetonitrile vs Ag/Ag^+ reference electrode; the originally reported potentials were recalculated with respect to SCE, using the standard reference electrode potentials tabulated by Pavlishchuk et al.[77]). The results clearly show that coordination of two amide groups decreases the redox potentials for the $Fe^{3+/2+}$ couple by at least 300 mV, thus indicating relative stabilization of the high oxidation state of iron center (the ratio of $K(Fe^{III}L)/ K(Fe^{II}L)$ increased by a factor of 10^8 for the macrocyclic diamide as compared to that for the macrocyclic amine). The acyclic analogues of H_2pydioneN_5 prepared and investigated by Mascharak and co-workers usually displayed even lower redox potentials for the $Fe^{3+/2+}$ couple, approaching −1 V versus SCE.[9] The difference in the iron(III) spin state and the geometric

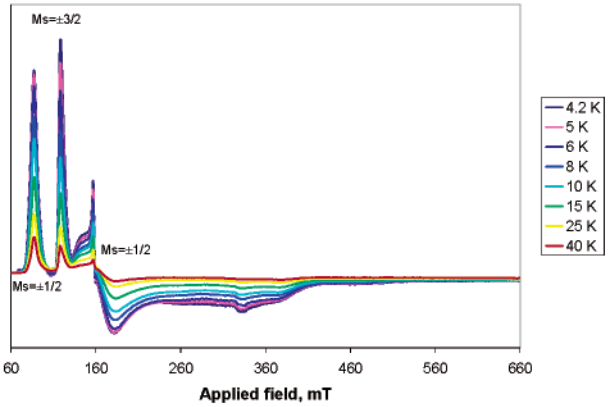

Figure 5. X-band EPR spectrum of **2**, frozen glass (MeOH/EtOH 1:1) at variable temperatures from 4.2 to 40 K. Spectrometer parameters: 0.1 mW of 9.3831 GHz radiation, modulation amplitude 1 mT, modulation frequency 100 kHz.

Scheme 3. Negative Axial Zero Field Splitting for Spin Sextet Fe^{III} (E/D = −0.08)

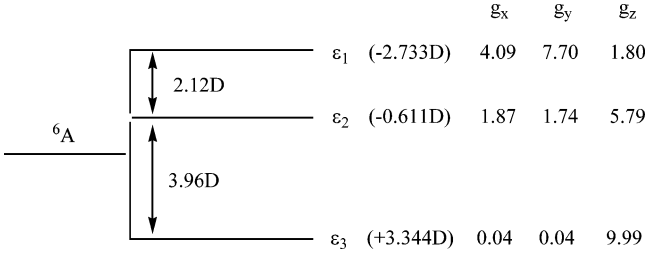

constraints of the macrocyclic ligand structure may account for the less dramatic influence of the amide donors on the redox stability of the +3 oxidation state of iron in its complex with H_2pydioneN_5.

EPR. Unlike most previously studied amide complexes of iron(III), which contained low-spin central metal ion and gave rise to EPR signals with $g \approx 2$,[7−9,12−18] complex **2** contains high-spin iron(III), as can be clearly seen from its characteristic EPR spectrum (Figure 5). Interestingly, even addition of cyanide or 1-methylimidazole does not convert iron into low-spin state; the complexes remain high-spin.

Anisotropic EPR spectrum of frozen solution of **2** in EtOH/MeOH mixture (Figure 5) is practically identical to the spectrum of a solid sample of **2** at 4.2 K. Consequently, the coordination environment of iron(III) determined by X-ray crystallography is retained in alcohol solutions.

The signal at g = 7.77 as well as broad signals at $g \sim$ 4.05 and 1.8 correspond to $M_s = \pm 1/2$ Kramers doublet, the signal at g = 5.70 arises from $M_s = \pm 3/2$ Kramers doublet, and a very weak signal at g = 9.7 ± 0.2, which could be observed at low temperature, originates from $M_s = \pm 5/2$ Kramers doublet (Scheme 3). The plots of effective g values versus E/D[78] allowed us to determine an E/D value of 0.08 for complex **2**, which corresponds to a distorted axial system.[79] As follows from the temperature dependence of the EPR spectra (intensities of the $M_s = \pm 3/2$ and $\pm 1/2$

(76) Ferraudi, G. *Inorg. Chem.* **1980**, *19*, 438−444.
(77) Pavlishchuk, V. V.; Addison, A. W. *Inorg. Chim. Acta* **2000**, *298*, 97−102.
(78) Wickman, H. H.; Klein, M. P.; Shirley, D. A. *J. Chem. Phys.* **1965**, *42*, 2113−2117.
(79) Solomon, E. I.; Brunold, T. C.; Davis, M. I.; Kemsley, J. N.; Lee, S.-K.; Lehnert, N.; Neese, F.; Skulan, A. J.; Yang, Y.-S.; Zhou, J. *Chem. Rev.* **2000**, *100*, 235−349.

transitions increase with temperature), the sign of D is negative. The temperature dependence of the EPR spectrum of **2** is represented in Figure 5.

A standard spin-Hamiltonian for the $S = 5/2$ system is[59]

$$H = g\beta BS + D[S_z^2 - S(S+1)/3] + E[S_x^2 - S_y^2] \quad (2)$$

where g is the electron g-factor, β is the Bohr magneton, D and E are axial and rhombic zero-field splitting constants, respectively, B is applied magnetic field, and S_i are the operators for electron spin angular momentum. For the purely axial case and negative value of D (under condition $|D| > h\nu$, at X-band $h\nu \approx 0.3$ cm^{-1}), the energy levels are presented in Scheme 3.

The corresponding eigenfunctions are[59]

$$|\phi_1^{\pm}\rangle = 0.9859|\pm 1/2\rangle + 0.1620|-3/2\rangle + 0.0411|\pm 5/2\rangle$$

$$|\phi_2^{\pm}\rangle = 0.9868|-3/2\rangle - 0.1565|\pm 1/2\rangle - 0.0465|\pm 5/2\rangle$$

$$|\phi_3^{\pm}\rangle = 0.9866|\pm 5/2\rangle - 0.0464|-3/2\rangle - 0.1565|\pm 1/2\rangle$$

To find the value of D, variable-temperature EPR experiments were conducted. The intensities of the EPR signals of the complex **2** obtained by double integration of the signals in EPR spectra were approximated by the equation[80−82]

$$N = N_0 A T^{-1}[1 + \exp(-3.96D/kT) + \exp(-6.08D/kT)]^{-1} \quad (5)$$

where k is the Boltzmann constant, N is the signal intensity, N_0 is the fitted parameter (a coefficient necessary to relate observed relative value of intensity to the calculated one), $A = 1$ for the ground $M_s = \pm 5/2$ state, $A = \exp(-3.96D/kT)$ for the $M_s = \pm 3/2$ excited state, and $A = \exp(-6.08D/kT)$ for the $M_s = \pm 1/2$ excited states. T^{-1} accounts for dependence of signal intensity on temperature; the other part describes the Boltzmann distribution of spin between the states.

The fit of the intensities of the signal at $g = 5.7$ (which corresponds to $M_s = \pm 3/2$) is presented in Figure 6. The corresponding absolute value of D is 0.5 cm^{-1}. A very close (identical within experimental error) value of D was also obtained by fitting the intensities of the signal with $g = 7.7$ (Supporting Information, Figure S7). The simulated EPR spectrum for **2** that was obtained with the values of spin-Hamiltonian parameters reported above, agrees well with the experimental spectrum and reproduces all its important features (Figure S1, Supporting Information).

The absolute value of D for the complex [Fe(pydioneN_5)-Cl(H_2O)] ($D = -0.5$ cm^{-1}) is very similar to the value reported for the analogous complex with an imine macrocycle [Fe(pydieneN_5)Cl_2]$^+$ ($D = +0.5$ cm^{-1}),[83,84] reflecting similarities in the electronic structure of both complexes with pentadentate aza-macrocycles.

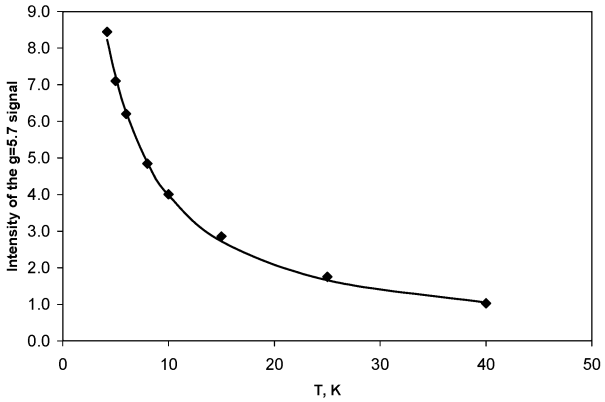

Figure 6. Nonlinear fit of the temperature dependency of double integral of EPR signal at $g = 5.7$. Dots represent the experimental values; the fit (eq 5) is shown by a solid line.

Mössbauer and Magnetic Susceptibility Measurements. The ambient temperature Mössbauer spectrum of **2** (Figure 7) consists of a single quadrupole doublet, indicating the presence of only one type of iron center in the solid state. The isomer shift ($\delta = 0.65$ mm/s at 1.2 K) and quadrupole splitting ($\Delta E_Q = 1.05$ mm/s at 77.5 K) values are consistent with the local seven-coordinate (pentagonal bipyramidal) high-spin iron(III) chromophore established by the single-crystal X-ray structure determination. It is difficult to obtain a reliable ambient temperature value for δ directly owing to relaxation broadening of this spectrum. However, the value calculated from the quadrupole shifted Zeeman pattern at 1.2 K extrapolates to ~0.5 mm/s (on correction for the second order Doppler shift ~+0.14 mm/s) and is typical of spin sextet ground-state Fe^{3+}. The Mössbauer parameters for **2** are generally similar to the values determined previously for seven-coordinate high spin iron(III) complexes with pydiene N_5.[85] Somewhat higher values of δ and ΔE_Q for [Fe(pydioneN_5)Cl(H_2O)] (see above) as compared to those for [Fe(pydieneN_5)Cl_2](ClO_4)$_4$ ($\delta = 0.41$ mm/s, $\Delta E_Q = 0.20$ mm/s, [85]) are consistent with greater σ-donor ability of the amide-containing ligand with respect to its Schiff base counterpart.

The temperature dependence of the zero field Mössbauer spectra of **2** is shown in Figure 7. The observed behavior is typical of high-spin iron(III) undergoing slow paramagnetic relaxation/broadening with decreasing temperature. Note the near complete disappearance of the high velocity component of the spectrum in the ±4 mm/s velocity sweep spectra of the left side of the figure. The ratios Γ_-/Γ_+ and A_-/A_+ are ~0.6 and ~1.1, respectively, at 293 K and ~0.6 and ~1.0 at 77.5 K, indicating that the spectral amplitude asymmetry is not the result of (significant) anisotropy of the recoil free fraction.[86] To the contrary, the temperature-dependent behavior is the result of a combination of negative single-ion zero-field splitting of the system's ground sextet and the self-

(80) Hammarberg, T.; Kuprin, S.; Radmark, O.; Holmgren, A. *Biochemistry* **2001**, *40*, 6371−6378.
(81) Scholes, C. P.; Isaacson, R. A.; Feher, G. *Biochim. Biophys. Acta* 1971, *244*, 206−210.
(82) Slappendel, S.; Veldink, G. A.; Vliegenthart, J. F. G.; Aasa, R.; Malmstrom, B. G. *Biochim. Biophys. Acta* 1980, *624*, 30−44.
(83) Cotton, S. A. *Chem. Phys. Lett.* **1976**, *41*, 606−608.
(84) Scoville, A. N.; Reiff, W. M. *Inorg. Chim. Acta* **1983**, *70*, 127−131.
(85) Deeney, F. A.; Nelson, S. M. *J. Phys. Chem. Solids* **1973**, *34*, 277−282.
(86) Buckley, A. N.; Herbert, I. R.; Rumbold, B. D.; Wilson, G. V. H.; Murray, K. S. *J. Phys. Chem. Solids* **1970**, *31*, 1423.

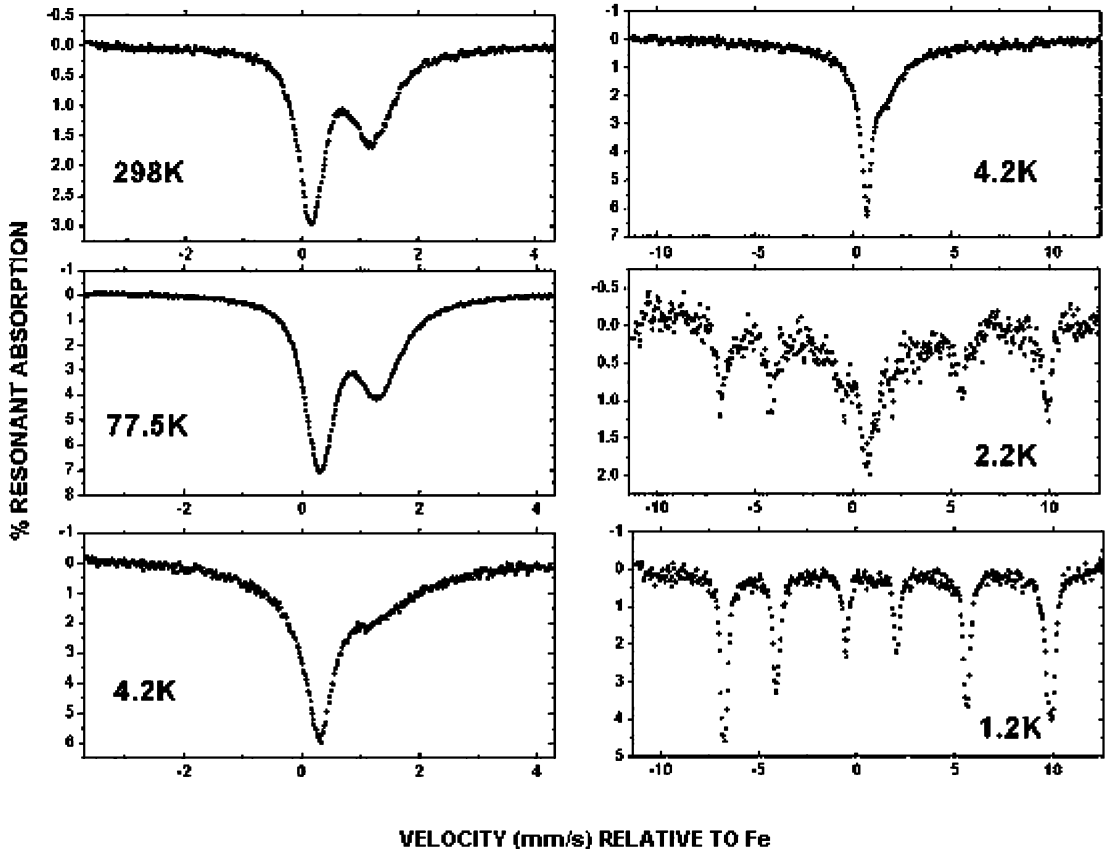

Figure 7. Temperature dependence of the Mössbauer spectra of **2**.

dilute nature of the compound leading to slow single ion relaxation. The former is suggested by the temperature dependence of the EPR spectrum (vide supra) as well as the Mössbauer spectra. $D < 0$ leads to a progressively increasing Boltzmann population of the slowly relaxing ground $M_S = \pm 5/2$ Kramers doublet and in the limit of infinitely slow relaxation a large internal hyperfine field (H_n) which in the present case is 51.7 T. This value was determined from the $I = 1/2$ (ground state) nuclear Zeeman splitting, which is either of Δ_{2-4} or Δ_{3-5} of the quadrupole-shifted hyperfine pattern from which $H_n = \langle \Delta_{2-4}$ or $\Delta_{3-5} \rangle / 0.1188$ (in Tesla).[87] The dilute nature is evidenced by a shortest inter complex $Fe^{III}-Fe^{III}$ distance of ~8 Å, a magnitude which previous detailed study[88] has shown to be large enough as to result in long spin−spin relaxation times for high-spin iron(III).

The local ligand chromophore of **2** is pentagonal bipyramidal $\{FeN_5ClO\}$. In this situation, one predicts $V_{zz} > 0$, i.e., stronger in-plane ligation than axial,[89] using a simple point charge model for calculation of the principal component of the electric field gradient tensor.[90] $V_{zz} > 0$ corresponds to $E_\sigma < E_\pi$, where the σ quadrupolar transition is $|1/2, \pm 1/2\rangle \rightarrow |3/2, \pm 1/2\rangle$ and π is $|1/2, \pm 1/2\rangle \rightarrow |3/2, \pm 3/2\rangle$. The theory[91] appropriate to the slow paramagnetic relaxation of an internal field longitudinal (parallel) to the principal axis of (a nonfluctuating) electric field gradient tensor (in the present case presumably the Cl−Fe−O nominal C_5 axis of **2**) predicts that the π transition should suffer the initial and largest line width broadening effect with the onset of slow paramagnetic relaxation. This is fully consistent with our observations and $V_{zz} > 0$. For the specific case of an axial quadrupole interaction that is smaller than the magnetic hyperfine interaction, the quadrupolar shift of the nuclear Zeeman spectrum, $S_1 - S_2 = -\Delta E(3 \cos^2 \theta - 1)$, where $S_1 = \Delta_{1-2}$, $S_2 = \Delta_{5-6}$ (from the spectrum at 1.2 K, Figure 7), ΔE is the limiting quadrupole splitting of the rapidly relaxing paramagnetic phase, and θ is the angle between V_{zz} and H_n. The foregoing equation[90] has a unique solution for θ when $S_1 - S_2 > \Delta E$ and from our data $\theta \sim 19°$, i.e., H_n is relaxing more or less parallel to V_{zz}. Furthermore, when $S_1 - S_2$ is negative and of absolute value greater than ΔE, as for the present complex, V_{zz} is positive. Thus, we have an internally consistent picture of the aspects of the local bonding and relaxation dynamics in this complex.

In summary, the slow paramagnetic relaxation behavior of the present complex is strongly reminiscent of that previously observed for certain trigonal planar (3 coordinate)[92,93] and trigonal bipyramidal (5 coordinate)[94,95] com-

(87) van Bongen Torman, J.; Jagannathan, R.; Trooster, J. M. *Hyperfine Interact.* **1975**, 1.
(88) Wignal, J. W. G. *J. Chem. Phys.* **1968**, *44*, 2462.
(89) Gibb, T. C. *Principles of Mössbauer Spectroscopy*; Chapman and Hall: London, 1976.
(90) Reiff, W. M. *Coord. Chem. Rev.* **1973**, *10*, 37.
(91) Blume, M.; Tjon, J. A. *Phys. Rev.* **1968**, *165*, 446.
(92) O'Donoghue, M. B.; Davis, W. M.; Schrock, R. R.; Reiff, W. M. *Inorg. Chem.* **1999**, *38*, 243−252.
(93) Fitzsimmons, B. W.; Johnson, C. E. *Chem. Phys. Lett.* **1974**, *24*, 422.
(94) Drummond, J.; Wood, J. S. *Chem. Commun.* **1969**, 1373.
(95) Reiff, W. M.; Wong, H.; Tuiroc, M.; Eisman, G. *J. Phys. Colloq.* **1979**, *40(C2)*, 237.

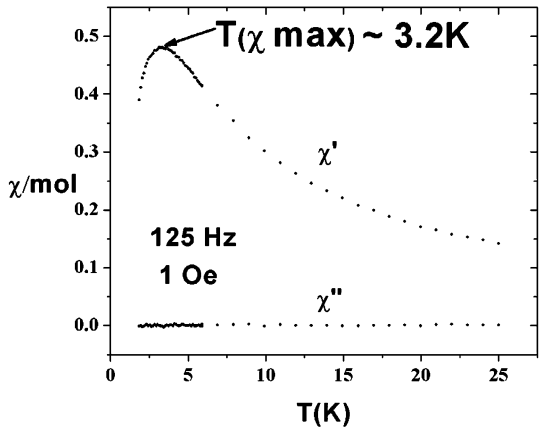

Figure 8. Temperature dependence of the ac susceptibility of **2**.

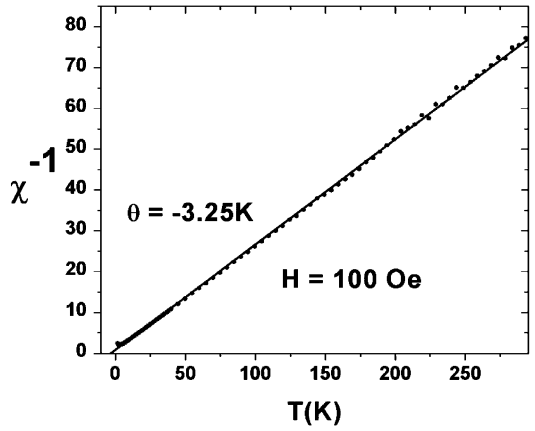

Figure 9. Temperature variation of the inverse susceptibility for **2**.

plexes of high-spin iron(III), as well as several pentagonal bipyramidal (seven-coordinate) complexes with pydieneN_5 in the equatorial plane, and halide or pseudohalide anions in the axial positions.[85] However, the foregoing three- and five-coordinate systems are nevertheless simple paramagnets at low temperatures, while there have been no detailed susceptibility studies of the mononuclear pydieneN_5 complexes below ~95 K.[30,85] On the other hand, the bulk ac and dc magnetization study of **2** gives clear and unequivocal evidence of a novel additional feature, namely an unexpected crossover to long-range (3D) magnetic order from slowly relaxing (paramagnetic) state that is now considered.

The temperature dependence of the ac susceptibility of the complex **2** is given in Figure 8. The room-temperature magnetic moment (5.84 μ_β) is consistent with a high-spin configuration of iron(III) in the complex [Fe(pydioneN_5)-Cl(H_2O)] with some reduction relative to the spin only value (5.92 μ_β) via weak AF exchange. The behavior of χ' and χ'' indicates collinear Néel antiferromagnetism with $T_N \sim 3.2$ K. A similar conclusion is obtained for low field dc SQUID magnetometry investigation which exhibits no magnetization dispersion for field and zero field cooled determinations, i.e., there is no canting. The overall moment decrease corresponding to the temperature variation of the χT product is large: ~3.4 μ_β (5.84 μ_β to 2.4 μ_β) over the range 293−1.8 K. The limiting value of 2.4 μ_β is considerably less than that expected[96] (≥4.4 μ_β, depending on the sign of D), for simple axial or near-axial single-ion field zero-field splitting effects and implies relatively strong antiferromagnetic exchange interactions between metal chromophores. The temperature variation of the inverse susceptibility, Figure 9, obeys a single Curie−Weiss law quite well over entire temperature range shown. As expected, fits (Figure 10) of the temperature variation of the magnetic susceptibility based entirely on single ion zero-field splitting and the parameters from Scheme 3 for a simple paramagnet fail to account for a presence of a maximum at 3.2 K. Moreover, the observed deviation of dependence of magnetic susceptibility on temperature ($\chi_{calculated} > \chi_{observed}$) is clearly typical of antiferromagnetic exchange interaction. This combined with the fact that the value of the paramagnetic Curie temperature,

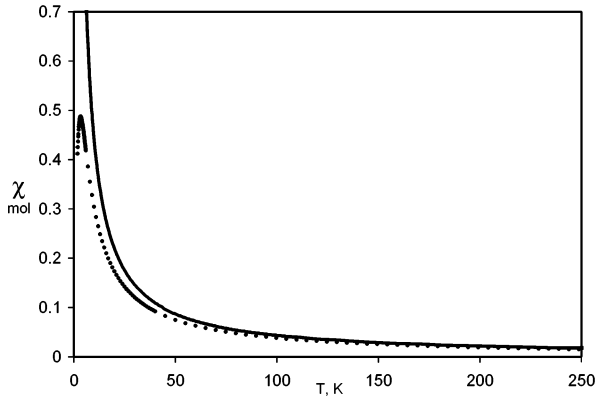

Figure 10. Temperature dependence of the ac susceptibility of **2**; dots represent experimental values, and solid line represents simulation based on the parameters from Scheme 3 ($D = -0.5$ cm^{-1}, $E/D = 0.08$, $g = 2.00$) for a simple single-ion paramagnet.

θ, is essentially identical to the value of T_N strongly suggests genuine three-dimensional magnetic order. There are no obvious 1D or 2D magnetic exchange effects in χ versus T. This is consistent with the 3D hydrogen bonded network structure depicted in the packing diagram of Figure 3 wherein there are no obvious 1D or 2D magnetic exchange pathways. An antiferromagnet of this type, i.e., one in which exchange interactions are more important than anisotropy effects (a situation fairly typical of ^{6}A ground-state Fe^{III} or Mn^{II} based magnets) or alternatively expressed as magnetic fields, one with H (exchange) > H (anisotropy),[97] should exhibit a first-order spin flop transition in its H versus T phase diagram for isothermal dc or ac magnetization at some $T < T_N$. Precisely this effect[98,99] is seen in the field dependence of the in phase (ac) susceptibility (Figure 11) at 1.85 K where the spin flop is centered at ~1.1 T for the polycrystalline powder. In passing, it should be noted that this field induced magnetic transition is typically not as obvious in the field dependence of the dc magnetization of a polycrystalline powder. In any event, the behavior exhibited in Figure 11 incontrovertibly further establishes a novel crossover to a

(96) Kotani, M. *Suppl. Prog. Theor. Phys.* **1966**, *17*, 4.

(97) Carlin, R. L.; van Duyneveldt, A. J. *Magnetic Properties of Transition Metal Compounds*; Springer-Verlag: New York, 1977.

(98) van Duyneveldt, A. J. *J. Appl. Phys.* **1982**, *53*, 8006.

(99) Manson, J. M.; Huang, Q.-z.; Lynn, J. W.; Koo, H.-J.; Whangbo, M.-H.; Bateman, R.; Otsuka, T.; Wada, N.; Argyriou, D. N.; Miller, J. S. *J. Am. Chem. Soc.* **2001**, *123*, 162−172.

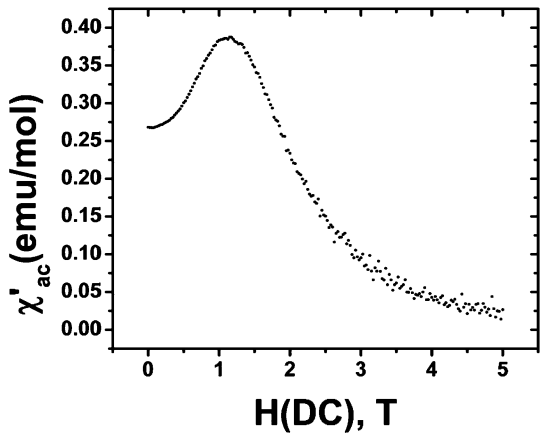

Figure 11. dc field dependence of the ac magnetization for **2**. Data points were collected every 0.025 T at 1.8 K, applying ac field of 2.5×10^{-4} T amplitude at a frequency of 500 Hz.

long-range ordered antiferromagnetic ground state for $T <$ ~3.2 K. It seems clear that detailed ac and dc magnetization study of **2** are indispensable to a complete understanding (save for additional single crystal studies) of its magnetic ground state. This is especially the case in light of the fact that limiting low temperature (zero field) Mössbauer spectra for the extremes of long-range order (at magnetic saturation) versus slow paramagnetic relaxation (in the infinitely slow relaxation limit) are virtually indistinguishable. We hasten to point out that these limiting behaviors can be distinguished using Mössbauer spectroscopy by analysis of the temperature dependence of the spectra using theory established by Blume[91] versus classic molecular field theory.[100,101] This laborious analysis, however, is not necessary in light of the detailed complimentary magnetization studies presented herein. Furthermore, the line shape at higher T and general lack of temperature variation in the magnitude of the internal field when resolved at low T are unambiguously consistent with slow single ion paramagnetic relaxation over essentially all of the temperature range investigated. The crossover to the ordered state occurs only at the lowest temperatures and is not readily apparent in the zero-field Mössbauer spectra.

Summary

A new, stable iron(III) complex with a pentadentate amide-containing ligand H_2pydioneN_5 was prepared and fully characterized. The set of donor atoms provided by H_2pydioneN_5 contains one pyridine nitrogen, two nitrogen atoms from deprotonated amide groups, and two secondary amines and is similar to that of bleomycin (pyrimidine, amide, imidazole, and two amines)[1−3] and many of previously synthesized bleomycin models.[69,102] The macrocyclic structure of the ligand H_2pydioneN_5, however, enforced planar arrangement of the five donor atoms, thus yielding a pentagonal-bipyramidal complex, in which an equatorial plane is occupied by the cyclic amidopyridine, and two axial positions are available for monodentate ligand coordination. The coordination of strongly electron-donating, negatively charged deprotonated amide groups resulted in expected stabilization of a high oxidation state of iron (the redox potential of the $Fe^{III}L/Fe^{II}L$ couple, −0.57 V versus SCE, was found to be ca. 300 mV more negative than the potential of the related pentaaza complex $[Fe(pyane N_5)Cl_2]^+$ that lacks amide groups[31]). In contrast to the majority of the iron complexes with polydentate amide ligands, which are usually low-spin,[69] the pentagonal-bipyramidal geometry of the macrocyclic complex $[Fe(pydione N_5)Cl(H_2O)]$ affords a high-spin configuration of the central metal ion. The amidopyridine macrocycle described in this work opens an access to high-spin, high oxidation state iron compounds with unusual redox properties which are currently being investigated. Additionally, the macrocyclic pentaaza-amidopyridine platform is promising for design and synthesis of magnetically coupled materials. Due to the presence of a rigid structural motif that contains two amide groups conjugated with an aromatic pyridine ring, the entire macrocycle adopts an essentially planar conformation in its crystallographically characterized iron(III) complex. The rigid, planar building blocks in $[Fe(pydione N_5)Cl(H_2O)](MeOH)$ are linked in a three-dimensional network via a system of hydrogen bonds. Significantly, the H_2pydioneN_5 ligand contains both hydrogen-bond donors (secondary amino groups) and hydrogen-bond acceptors (oxygen atoms from the amide carbonyls) and participates in a number of H-bonding interactions through the solvent molecules (water or methanol). Even though the metal−metal separations in crystalline complex $[Fe(pydione N_5)Cl(H_2O)](MeOH)$ are relatively large (8.02 Å), the material exhibits antiferromagnetic ordering below 3.2 K. In the future studies, long-range magnetic ordering through the hydrogen bond network can be enhanced by much stronger coupling via bridging monodentate ligands.

Acknowledgment. This research was supported by the NSF (CHE 0111202) and the Research Corporation (RI0223). The CCD based X-ray diffractometer at Harvard University was purchased through an NIH grant (1S10RR11937-01). The NMR facility in the Chemistry Department at Tufts University is supported by NSF Grant CHE-9723772. The EPR facility at Tufts is supported by the NSF (CHE 9816557). Authors thank Dr. Ralph Weber (Bruker-Biospin) for his help in acquiring low temperature EPR spectra, Dr. Samuel Kounaves for access to some of electrochemical instrumentation, Dr. Terry E. Haas and Dr. Regina Valluzzi for their help in acquiring X-ray powder diffraction data, and Dr. Karsten Meyer (University of California, San Diego) for providing software for EPR simulations. Finally, ac susceptometry and dc/ac SQUID magnetometry instrumentation at Northeastern University were purchased through partial support of NSF instrumentation grants. Authors would like to thank anonymous reviewers A and E for their helpful suggestions.

(100) Wertheim, G. K.; Guddenheim, H. J.; Buchanan, D. N. E. *Phys. Rev.* **1968**, *169*, 465−470.
(101) Kadanoff, L. P.; Gotze, W.; Hamblen, D.; Hecht, R.; Lewis, E. A. S.; Palciaus, V. V.; Rayl, M.; Swift, J.; Aspnes, D.; Kane, J. *Rev. Mod. Phys.* **1967**, *39*, 395.
(102) Huang, L.; Quada, J. C., Jr.; Lown, J. W. *Curr. Med. Chem.* **1995**, *2*, 543−560.

Supporting Information Available: X-ray crystallographic files in CIF format for **1** and **2**. X-ray powder diffraction data for **2**. Plots of linear variation of i_p with $v^{1/2}$ for electrochemical oxidation of **2**, plot of simulated EPR spectrum of **2**, plot of nonlinear fit of dependency of EPR signal intensity at $g = 7.7$ on temperature for **2**, UV−vis spectra of **2** recorded at different temperatures. This material is available free of charge via the Internet at http://pubs.acs.org.

IC0351601